An Analysis of Atlantic Tropical Cyclone Motion from 1988 to 2014

By: Chelsey Nakita Laurencin

Abstract

In this study, we examine the seasonal and interannual variability of the North Atlantic (NATL) tropical cyclone (TC) motion from the historical Hurricane Database (HURDAT2) over the period 1988-2014. We characterize these motions based on their position, lifecycle, and seasonal cycle. The main findings of this study include: 1) Of the 11,469 NATL TC fixes examined between 1988-2014, 81% of them had a translation speed of < 20mph; 2) TCs in the deep tropics of the NATL are invariably slow-moving in comparison to TCs in higher latitudes. Although fast moving TCs (> 40 mph) are exclusively found north of 30N, the slow moving TCs have a wide range of latitude. This is largely a consequence of the background steering flow being weaker (stronger) in the tropical (higher) latitudes with a minimum around the subtropical latitudes of NATL; 3) There is an overall decrease in the frequency of all categories of translation speed of TCs in warm relative to cold El Niño Southern Oscillation (ENSO) years. However, in terms of the percentage change, TCs with a translation speed in the range of 10-20 mph display the most change (42%) in warm relative to cold ENSO years; and 4) There is an overall decrease in frequency across all categories of TC translation speed in small relative to large Atlantic Warm Pool years, but in terms of percentage change in the frequency of TCs, there is significant and comparable change in the frequency over a wider range of translation speeds than the ENSO composites. This last finding suggests that Atlantic Warm Pool variations have a more profound impact on the translation speed of Atlantic TCs than ENSO.

TABLE OF CONTENTS

LIST OF FIGURES

1. INTRODUCTION

Description of Tropical Cyclone Motion

Tropical cyclones (TCs) are important in redistributing the surplus heat from the equator to the poles, helping to modulate global temperatures (NOAA 2016). However, they are also the cause for some of the most expensive collateral damages and human mortality when they make landfall. The primary feature that steers TCs is the large scale surrounding environmental flow within the troposphere (George and Gray 1976; Holland 1983; Elsberry 2005; Colbert and Soden 2012; Mei et al. 2014). Other influences on TC motion include the latitudinal variation of the Coriolis parameter f (= $2\Omega\sin\varphi$) and thus absolute vorticity, location and orientation of the TC β-gyres, vertical wind shear (UCAR 2016), and the non-uniform vertical structure of the storm (UCAR 2016; Elsberry 2005). The meridional change in f results in a weak northwestward force on TCs, known as the β effect (Chan 2005; Elsberry 2005). The β effect is associated with stronger tangential winds and relative vorticity to the northeast quadrant of the vortex, known as β-gyres. However, the outer structure of the cyclone impacts how strong the β effect's northwestward displacement is (Chan 2005; Elsberry 2005). Additionally, forecasted cyclone position is directly related to predicted location of maximum relative vorticity (Chan 1984), meaning that cyclones are more likely to travel to locations where their vorticity would be maximum.

Tropical Cyclones in the Atlantic

In the Atlantic, there has been a sharp increase in the number of tropical cyclones since the mid-1990s (Mei et al. 2014). The behavior and activity of the cyclones here is related to

different climatic anomalies such as the El Niño-Southern Oscillation (ENSO) and the Atlantic Warm Pool (AWP; Wang and Enfield 2001). The Atlantic also has the highest number of recurving tropical cyclones than any other basin. Primarily, this is due to the North Atlantic Subtropical high (NASH; Colbert and Soden 2012). When TCs develop on the southeastern corner of the NASH, they are pushed westward and depending on the strength of the NASH, will either advance to landfall or recurve to ocean. A weak NASH retreats northeastward, by which TCs are steered westward along its equatorward edge and recurve back northeastward on the poleward side of the NASH. When the NASH is strong, it extends westward, by which TCs are more likely to develop as recurving landfall TCs (Wang et al. 2011; Colbert and Soden 2012). The farther west that a hurricane develops, the less likely the cyclone will recurve back toward the ocean as it has less time to do so before reaching land. Ultimately, the recurvature of cyclones in the Atlantic is a byproduct of the position and strength of the NASH as well as the development location of the hurricane (Elsner et al. 2003).

2. LITERATURE REVIEW

Previous research has been conducted on topics involving TC motion. A study conducted by Colbert and Soden (2012) analyzed relationships between environmental steering flow and TC tracks. This study revealed that in the Atlantic, TC tracks are directly influenced by the location and intensity of the subtropical high: straight-moving and recurving landfall TCs are associated with a westward extension and intensification of the subtropical high, whereas recurving ocean storms are associated with the subtropical high's weakening and northeastward retreat (Colbert and Soden 2012). They also investigated the relationship between TC tracks and the El Niño Southern Oscillation. They showed that the ENSO-forced modulation of the NASH

had a consequent influence on the Atlantic TC tracks. For example, the weakening of the NASH during warm ENSO events led to an increase in the likelihood of TCs in the Atlantic to recurve out to the ocean. Similarly, they showed that during cold ENSO events, TCs traveled farther west than during warm ENSO events.

It is important to note, however, that Colbert and Soden (2012) only considered TCs that developed in the MDR. In this study, we include all Atlantic TC development locations included in the National Hurricane Center's HURDAT dataset from 1988 to 2014. Furthermore, Colbert and Soden (2012) analyzed a larger time period (1950 to 2010) than the time period examined in this study. It is also noteworthy that while the Beta and Advection Model (BAM) used in their study generally provided comparable simulated TC tracks to the actual tracks, small directional biases did develop, slightly affecting the accuracy in their data.

It is important to reference the impact of ENSO, the anomalous warming and cooling of equatorial Pacific Ocean waters, on TC Motion. The warm phase of ENSO is referred to as El Niño, during which waters in the equatorial Pacific maintain a SST mean 0.5°C warmer than average for three consecutive months. When the three month running mean is 0.5°C cooler than average, it is referred to as a La Niña event (CPC 2016). When ocean temperatures are neither 0.5°C warmer or cooler than average, it is considered to be a neutral year. Generally, an El Niño event reduces the occurrence of cyclones in the Atlantic while La Niña favors cyclone development (Bove et al. 1998). Based on the work of Bove et al. (1998), there is a 28% chance of two or more hurricanes making landfall in the US during El Niño, while there is a 66% chance during La Niña. The probability is similar for major hurricanes (at least 111 mi/hr sustained winds), with a 23% chance of a major hurricane making US landfall during El Niño and a 63% chance during La Niña (Bove et al. 1998). This lines up with previous work done on TC motion,

where it was found that El Niño events are associated with a weakening of NASH, resulting in fewer landfalling TCs during this phase of ENSO (Xie et al. 2005; Kossin et al. 2010; Wang et al. 2011; Colbert and Soden 2012).

The Atlantic Warm Pool (AWP) also plays a role in TC activity. The AWP is a warm body of water comprising the Caribbean Sea, Gulf of Mexico, and the Western North Atlantic Ocean (Misra et al. 2015). This region is delineated by the 28.5℃ isotherm in SST, by which the area within this region exhibits interannual fluctuations (Wang et al. 2006; 2011; Misra et al. 2015). When the AWP area is large (small), the summertime NASH weakens (strengthens), retreating northeastward (southwestward). This suggests that the size of the AWP is indirectly related to the motion of Atlantic tropical cyclones through the NASH.

This study characterizes North Atlantic tropical cyclone (TC) translation in relation to the El Niño-Southern Oscillation (ENSO) and the Atlantic Warm Pool (AWP). In terms of the phase and magnitude of the ENSO and AWP, this research examines the relationship between TC translation speed and its lifetime and geographic location. It also surveys the connection that TC motion holds with prevailing steering flow under these conditions.

3. METHODOLOGY & DATA

Data

The data used to calculate the translation speeds of the tropical cyclones was obtained from Colorado State University's supplement to the National Hurricane Center's North Atlantic hurricane database (HURDAT): The Extended Best Track Dataset of Atlantic hurricanes from 1988 to 2014 (Demuth et al. 2004). HURDAT provides the data measurements in six hour

intervals. The parameters used from this dataset include latitude (°N), longitude (°W), time (UTC) and date every 6 hours. A cyclone's position, based on latitude and longitude coordinates is referred to as a "fix."

To observe the composite steering flow associated with the TCs in this study, the Climate Forecast System Reanalysis (CFSR; Saha et al. 2010) is used. This reanalysis is available from 1979-2010 at approximately 0.5° resolution globally at daily intervals. It is used to produce a composite of upper air circulation in order to view the steering flow conditions for the time period and conditions in review. Since SSTs also play a role in TC activity, we also generate composite SST maps from the Optimally Interpolated SST version 2 (OISSTv2; Reynolds et al. 2007), available from 1981 to the present. This data is presented at 1°×1° grid resolution in monthly intervals.

Methodology

The latitude and longitude coordinates of the TC fixes were used to calculate the changes in north-south (meridional) and east-west (zonal) speed components of the TC translation speed, respectively. Zonal changes are calculated by subtracting the TC's initial position from its final position, and continuing that trend for all longitude points provided for a specific hurricane. Thus, a westward moving storm would have a positive change in longitude, while an eastward-moving storm would have a negative change. Similarly, changes in the meridional direction are found by subtracting the cyclones initial from final position, so that a northward moving storm has a positive latitudinal change and a southward moving storm has a negative change.

Since this study deals with synoptic scales, the curvature of the Earth must be accounted for. The Earth is assumed to be a perfect sphere when calculating distances and speeds of the TCs. Thus, when converting the latitudinal and longitudinal changes from degrees to nautical

miles, the Earths average radius R_e is used (3440.065 nmi). Because lines of latitude do not converge when moving in the north-south direction, the distance between lines of latitude does not change. The following arc length formula is used in calculating latitudinal change, where $\Delta\varphi$ is the change in latitude, and ΔY is the tropical cyclone's latitudinal change every 6 hours in nautical miles:

$$\Delta Y = R_e \, \Delta\varphi$$

However, lines of longitude converge towards the poles, so the distance between lines of longitude is not constant when moving north and south. Thus, the distance between two lines of longitude depends on which latitude the TC is located at. Furthermore, the perpendicular distance from Earth's axis of rotation to a point on the surface is also latitude-dependent, generating a varying radius when calculating the east-west distance ΔX between two fixes. To find the latitude-dependent radius, the following formula is used, where R_{lat} is the latitude-dependent radius from the Earth's axis of rotation:

$$R_{lat} = R_e \cos(\varphi)$$

Now the arc length formula is applied, this time using the horizontal change in longitude $\Delta\lambda$ to find ΔX every 6 hours in nautical miles:

$$\Delta X = R_{lat} \, \Delta\lambda$$

Lastly, the translation speed of the TCs is calculated. To account for the Earth's sphericity, the haversine formula is employed. This formula provides the distance ΔS between two fixes, given their latitude and longitude coordinates:

$$\Delta S = 2R_e \sin^{-1}\left(\sqrt{\sin^2\left(\frac{\Delta\varphi}{2}\right) + \cos\varphi_1 \cos\varphi_2 \sin^2\left(\frac{\Delta\lambda}{2}\right)}\right)$$

Because ΔX, ΔY, and ΔS are all distances traveled over a 6-hour time period, they are essentially speeds with units of nautical miles per 6 hours. To gain a better sense of familiarity with the speeds, the units are converted to miles per hour.

In classifying the phases of the ENSO, we make use of the Niño3.4 SST anomalies (CPC 2016). Because the months of September and August have the maximum number of hurricanes and TC fixes throughout the Atlantic hurricane season, we consider an El Niño (La Niña) year as one in which the SST anomaly index is 0.5℃ or more (-0.5℃ or less) during both months. Years in which both August and September do not have SST departure of 0.5℃ greater than (less than) the three-month running mean are neutral. For the time period in review (1988-2014), there are a total of 5 El Niño events and 8 La Niña events. Therefore, to normalize the data, we consider the 5 warmest El Niño years (by default), along with the 5 coldest La Niña years (with the most negative SST anomalies). The anomalies along with their corresponding years can be found in Table 2. Refer to Figure 6 for a visual representation of the anomalous warming and cooling of the equatorial Pacific.

To distinguish between a large and small AWP year, we consider the areal mean of the AWP (delineated by the 28.5℃ isotherm) from 1988 to 2014. Years that fall in the top (bottom) quartile are classified as large (small) AWP years. Using this approach results in 7 large AWP years and 7 small AWP years. In calculating the AWP indices for each year, we consider the departure of each year's AWP area from the areal mean, from 1988 to 2014. Thus, the 7 largest years carry the highest indices, while the 7 smallest years hold the most negative indices over the

27-year period (Table 2). Neutral years are those during which, the area enclosed by the 28.5℃ isotherm is neither in the top nor bottom quartile.

4. RESULTS

Seasonality

It is well documented that the Atlantic hurricane season runs from June 1st to November 30th. The maximum frequency of Atlantic TCs occurs during September (Table 1). Climatologically, we see that the fastest-moving tropical cyclones occur during the months of September and October (Figure 1). This seasonal variation coincides with the seasonal peak of the stronger TCs (those with faster maximum sustained winds around the eyewall; UCAR 2016). In addition, September is also the month when Atlantic TCs are most likely to undergo extratropical transition and therefore maintain faster translation speeds (Jones et al. 2003). Thus, a substantial portion of the fixes during this month is expected to be extratropical cyclones or tropical cyclones that later re-intensify as extratropical systems.

The zonal and meridional components of TC speeds per month are also compared in Figure 1. Both components exhibit an increasing speed as the hurricane season progresses. However, disregarding outliers, the corresponding ΔX components are slightly faster than the ΔY components. This difference is more apparent earlier in the hurricane season during the months of June and July. This points to a slight east-west bias in the movement of tropical cyclones in the North Atlantic. Based on the results of Colbert and Soden's study, this slight bias may be related to the recurvature of the cyclones induced by the NASH (2012). The subtropical high retreats poleward and westward during the summer and early fall, which is essentially the Atlantic hurricane season (NCDC 2016). In the mid-latitudes, westerly winds prevail and in the

tropics, easterlies are more prominent, contributing more of a zonal than meridional preference to TC tracks. Further, the β-drift may also play a role in that it induces a slight westward movement of TCs.

Latitude and Longitude

Figure 2 displays the distribution of translation speed of the TCs with latitude. This figure shows that the maximum in TC translation speed is near 50 °N. In the Atlantic, this is the approximate latitude at which TCs have undergone extratropical transition (Jones et al. 2003). Extratropical cyclones are known to travel faster than tropical cyclones, so this data lines up with previously conducted research in this regard. Further, Figure 2 shows a decreased frequency of cyclones north of 50 °N, which can be explained by the fact that not all TCs evolve into storms with extratropical characteristics. The environment here is not conducive to tropical storm growth with the increased baroclinicity, wind shear, and reduced SSTs. In Figure 3, this data can again be seen as a function of both month and latitude. It shows that a maximum in translation speed occurs in the mid-latitudes and a relative maximum in the tropics, where the trade winds influence TC propagation speed. The most common TC speeds fall in the range of 10-20 mi/hr, followed by speeds less than 10 mi/hr (Figure 4). Because the frequency of TCs sharply declines with increasing speed, only the most frequent speed ranges (<10 mi/hr, 10-20 mi/hr, 20-30 mi/hr, 30-40 mi/hr) are used in examining the influence of climatological anomalies on TC translation speed.

ENSO Variations

It is well documented that ENSO has a strong influence on TC activity. Across all speed ranges, there is a decrease in frequency of TCs in warm ENSO years than during cold ENSO years

(Figure 5). This reduction is most apparent for the speed range of 10-20 mi/hr, with a net frequency decrease of 42%. This speed range also carries the largest sample size. The second largest decrease (19%) in frequency in warm relative to cold years is for TCs traveling 30-40 mi/hr, also the range with the smallest sample size. This is followed by decreases of 15% and 12% for <10 mi/hr and 20-30 mi/hr, respectively (Figure 5).

The changes for these speed ranges may be observed geographically with the track density (number of TCs per 2°×2° cell) plots in Figure 7. Slower speeds (<10 mi/hr) can be observed in the deep tropics and subtropics, while TCs generally travel faster in the mid latitudes. Cold ENSO years are more so associated with slower translation in the tropics, whereas warm ENSO years maintain slower translation in the subtropics (Figure 7a-c). It is interesting to note that for cold (warm) ENSO events, there are relatively higher track densities along concave coastlines in the deep tropics (subtropics; Figure 7a-c). Looking at speeds 10 – 20 mi/hr, we see that this trend continues to hold true, though with a decreased track density (indicating a lower frequency) in TCs for both cold and warm ENSO years. The relative maximum in track density for cold events in the speed range of 10-20 mi/hr can be explained through the Atlantic trade winds. According to Giannini et al., the trade winds are generally stronger during La Niña events, contributing an additional easterly component to TC translation (2000). However, there is a relative maximum in the 20-30 mi/hr track density in the south Caribbean Sea for warm years, compared to cold years (Figure 7i). It is possible that there are other influences on TC motion that could be responsible for this. Finally, for TCs traveling 30 – 40 mi/hr, much of the track density is in the mid-latitudes at significantly lower frequency than for <10 mi/hr (Figure 7j-l). Thus, a meridional difference is apparent in TC translation between the cold and warm phases of ENSO.

The composite steering flow from 1988 to 2014 can be used to understand where this difference in TC translation comes from. In this study, the steering flow is defined by the vertically averaged winds in the 850 and 200hPa layer (Dong and Neumann 1986; Wang et al. 2011). Figure 8 shows the climatological steering flow (Figure 8a) for the time period in review along with the composite for cold (Figure 8b) and warm ENSO years (Figure 8c), and their differences (Figure 8d-f). There is increased westerly flow during warm ENSO years, whereas the steering flow during cold years carries more of an easterly component (Figure 8d-e). This steering flow pattern results in conditions that are favorable for TCs to make landfall in the eastern US during cold years; it is unfavorable for landfall in warm years. This corresponds to the findings of Colbert and Soden (2012), who revealed that landfalling TCs are more common during cold ENSO than in warm ENSO years.

AWP Variations

As noted earlier, the extent of the AWP (delineated by the 28.5℃ isotherm) also plays a role on Atlantic TC motion. The composite SSTs for the large and small AWP phases and their difference is shown in Figure 10. While the anomalous warming and cooling are not as strong as it is for ENSO events (Figure 10c), the spatial extent of the AWP clearly varies from large to small years (Figure 10a-b). Similar to the frequency distribution for ENSO, large AWP years contain both a larger sample size and net increase in frequency than small AWP years (Figure 9). For both phases, the AWP exhibits a maximum in frequency for TCs traveling at 10-20 mi/hr. Figure 9 also shows that this speed range carries the largest decrease in frequency from large to small years, with a 42% change. However, the AWP has a smaller spread amongst frequency differences between the large and small phases than ENSO does (Figure 5c; 9c). In fact, the AWP frequency differences are all greater than or equal to the differences computed for the ENSO phases. This

suggests that the phase of the AWP has a stronger influence on TC translation across all speed ranges.

Looking at the composite track density plots (Figure 11), we see again see that the track density decreases with increasing speed for both large and small AWP years. Overall, the large AWP years maintain a higher track density than small years. This lines up with previous research in that a large AWP is associated with decreased vertical wind shear and increased SSTs, conditions favorable for TC development (Wang et al. 2011). For both phases, we also see relative maxima in track density along concave coastlines, more apparent in large than small AWP years (Figure 11a-c). The difference in track density across the phases of the AWP is noticeable in the east-west direction across all speed ranges (Figure 11c, f, i and l). For speeds <30 mi/hr, small AWP years have higher track densities than large years along the western Atlantic and southern Caribbean Sea. The low sample size for TCs traveling 30-40 mi/hr makes it difficult to observe the difference for this range. Since the 28.5℃ isotherm predominantly expands and contracts in the east-west direction, and warm SSTs boosts cyclogenesis, this data is reasonable. Moreover, the NASH is stronger during small AWP years. This means that it expands westward and strengthens the trade winds and Caribbean Low Level Jet, steering TCs farther westward toward the US eastern seaboard (Wang et al. 2006; 2011).

This phenomenon can be viewed by examining the composite steering flow in Figure 12. During small AWP years, we see an increased easterly flow relative to climatology south of 15°N, (Figure 12e), while an increased westerly flow is observed here for large AWP years relative to climatology (Figure 12d). Westerly flow south of 15 °N for large with respect to small years strengthens (weakens) in the western (eastern) Atlantic (Figure 12f). North of 25 °N, westerly flow for small years decreases with respect to climatology (Figure 12e). For large years relative to

climatology, westerly flow increases in the western Atlantic and then shifts to easterly flow in the eastern Atlantic (Figure 12d). The anomalous zonal steering flow differences in Figure 12 further display and parallel the east-west track density changes in translation speed that were discussed in the previous subsection.

5. CONCLUSION

This study has characterized North Atlantic TC motion based on the phase and magnitude of the El Niño Southern Oscillation and the Atlantic Warm Pool. The data used 27 years of 6-hourly TC fixes to gain insight on how TC translation is influenced by these anomalous variations. For both phenomena, a maximum in TC frequency occurs during the peak of the Atlantic hurricane season (September and October), with a decrease in TC frequency at higher latitudes. Over the 27-year period, faster translation speeds (>40 mi/hr) are observed north of 30°N. Climatologically, approximately 81% of the TCs maintain translation speeds <20 mi/hr, 18% have speeds in the range of 20 – 60 mi/hr, with the remaining 1% being extratropical cyclones traveling faster than 60 mi/hr.

In analyzing the ENSO's effects on TC translation, a net increase in TC frequency is observed in cold relative to warm ENSO years. For both phases, the highest frequency of TCs occurred in the speed range of 10 – 20 mi/hr. This range also showed the largest percent decrease (42%) in frequency from cold to warm years. This difference in frequency can be observed in the track density plots, which revealed a meridional change between the two phases. For translation speeds between <30 mi/hr, Cold ENSO years have higher track densities in the tropics, whereas warm years have higher track densities in the subtropics. Additionally, the steering flow patterns

present during cold (warm) years result in more (fewer) landfalling TCs in the US eastern seaboard.

An analysis of the AWP revealed a higher TC frequency in large AWP years than in small AWP years. Unlike ENSO, the decrease in frequency from large to small AWP years was similar over all four ranges. Approximately a 30% change was detected across the four speed ranges analyzed (<10 mi/hr, 10-20 mi/hr, 20-30 mi/hr, 30-40 mi/hr). This suggests that AWP has a stronger impact on TC translation than ENSO does. This influence occurs in the east-west direction, with a higher TC frequency in the eastern (western) Atlantic during large (small) AWP years. The associated steering flow contributes to this change in that increased tropical westerly flow occurs during large AWP years, while easterly winds prevail during small AWP years. The expansion and contraction of the 28.5℃ isotherm is linked to this flow, favoring cyclogenesis along its eastern boundary.

References

Bove, M. C., J. B. Elsner, C. W. Landsea, X. Niu, and J. J. O'Brien, 1998: Effects of El Niño on U.S. landfalling hurricanes, revisited. *Bull. Amer. Meteor. Soc.*, **79**, 2477–2482.

Chan, J. C.-L., 1984: An observational study of the physical processes responsible for tropical cyclone motion. *J. Atmos. Sci*., **41**, 1036-1048.

Chan, J. C.-L., 2005: The physics of tropical cyclone motion. *Ann. Rev. Fluid Mech*., **37**, 99-128.

Colbert, A. J., and B. J. Soden, 2012: Climatological variations in North Atlantic tropical cyclone tracks. *J. Climate*, **25**, 657 – 673.

CPC, 2016: Cold & Warm Episodes by Season. National Oceanic and Atmospheric Administration. [Available online at http://www.cpc.noaa.gov/products/analysis_monitoring/ensostuff/ensoyears.shtml.]

DeMaria, M., J. Pennington, and K. Williams, 2015: Description of the extended best track file. Colorado State University.

Dong, K. and Neumann, C.J. (1986) The Relationship between Tropical Cyclone Motion and the Environmental Geostrophic Flows. *Monthly Weather Review*, **114**, 115-122.

Elsberry, R. L., 2005: Tropical cyclone motion. University of Wisconsin – Milwaukee, 106 – 196.

Elsner, J. B., 2003: Tracking hurricanes. *Bull. Amer. Meteor. Soc*., **84**, 353–356.

Giannini, A., Kushnir, Y. and Cane, M.A. (2000) Interannual Variability of Caribbean Rainfall, ENSO, and the Atlantic Ocean*. *Journal of Climate*, **13**, 297-311.

George, J. E., and W. M. Gray, 1976: Tropical cyclone motion and surrounding parameter relationships. *J. Appl. Meteor*., **15**, 1252–1264, doi:10.1175/1520-0450(1976)015,1252: TCMASP.2.0.CO;2.

Holland, G. J., 1983: Tropical cyclone motion: Environmental interaction plus a beta effect. *J. Atmos. Sci.*, **40**, 328–342, doi:10.1175/1520-0469(1983)040,0328:TCMEIP.2.0.CO;2.

Jones, S. C., P. J. Harr, J. Abraham, L. Bosart, P. J. Bowyer, J. L. Evans, . . . and T. Thorncroft, 2003: The Extratropical Transition of Tropical Cyclones: Forecast Challenges, Current Understanding, and Future Directions. *Wea. and Forecasting*, **6**, 1052 – 1092.

Kossin, J.P., Camargo, S. J. and Sitkowski, M. (2010) Climate Modulation of North Atlantic Hurricane Tracks. *J. Climate*, **23**, 3057-3076.

Mei, W., S. Xie, and M. Zhao, 2014: Variability of Tropical Cyclone Track Density in the North Atlantic: Observations and High-Resolution Simulations. *J. Climate*, **27**, 4797 – 4814.

Misra, V., C. Wang, Y. Serra, K. Karnauskas, E. M. Ellinor, J. Sheinbaum, . . . and J. Ochoa, 2015: The Intra-Americas sea: A region of challenges and opportunities to understand North American climate variability and predictability. [Available online at [ftp://ftp.aoml.noaa.gov/phod/pub/sklee/iasclip/IASCLiP_White_Paper_2015.pdf.]

NCDC, 2016: Subtropical highs. National Oceanic and Atmospheric Administration. [Available online at https://www.ncdc.noaa.gov/monitoring-references/dyk/subtropical-highs.]

NOAA, 2016: Tropical cyclone introduction. [Available online at http://www.srh.noaa.gov/jetstream/tropics/tc.html.]

Reynolds, R.W., Smith, T.M., Liu, C., Chelton, D.B., Casey, K.S. and Schlax, M.G. (2007) Daily High-Resolution-Blended Analyses for Sea Surface Temperature. *J. Climate*, **20**, 5473-5496.

Saha, S. and Coauthors. (2010) The NCEP Climate Forecast System Reanalysis. *Bull. Amer. Meteor. Soc*., **91**, 1015-1097.

UCAR, 2016: Tropical Cyclones. *Introduction to Tropical Meteorology*, COMET Program.

Wang, C., and D. B. Enfield, 2001: The tropical western hemisphere warm pool. *Geophys. Res. Letters,* **28**, 1635 – 1638.

Wang, C., Enfield, D.B., Lee, S.-K. and Landsea, C.W. (2006) Influences of the Atlantic Warm Pool on Western Hemisphere Summer Rainfall and Atlantic Hurricanes. *Journal of Climate*, **19**, 3011-3028.

Wang, C., Liu, H., Lee, S.-K., and Atlas, R. (2011) Impact of the Atlantic warm pool on United States landfalling hurricanes. *Geophys. Res. Lett*ers, **38**, 1635-1638.

Xie, L., Yan, T., Pietrafesa, L.J., Morrison, J.M. and Karl, T. (2005) Climatology and Interannual Variability of North Atlantic Hurricane Tracks. *J. Climate*, **18**, 5370-5381.

APPENDIX

Month	Number of Fixes	Translation speed (mi/hr)		
		Total	Zonal	Meridional
June	461	13.9	9.2	8.6
July	1069	15.3	12.0	7.5
August	2805	14.7	11.5	7.0
September	4414	13.7	9.8	7.6
October	2036	13.6	9.5	7.8
November	684	13.8	9.6	8.1

Table 1: The number of TC fixes and their mean climatological translation speed by month from the Extended Best Track (EBT; Demuth et al. 2014) data for the 1988-2014 period (Demuth et al. 2004).

Commented [LC1]: Get clarification on this reference and insert in reference list

Warm ENSO years	Cold ENSO years	Large AWP years	Small AWP years
1991 [0.8]	1988 [-1.3]	1998 [1.5]	1988 [-1.4]
1997 [1.8]	1998 [-1.0]	2005 [1.8]	1989 [-2.0]
2002 [1.0]	1999 [-1.1]	2009 [1.2]	1991 [-2.3]
2004 [0.6]	2007 [-0.8]	2010 [2.7]	1992 [-2.7]
2009 [0.7]	2010 [-1.2]	2011 [1.2]	1994 [-1.7]
		2012 [1.2]	2000 [-1.2]
		2014 [1.2]	2001 [-1.2]

Table 2: The years used in making composites of TC translation speeds for the warm and cold ENSO years and large and small AWP years are indicated. The magnitude of the Niño3.4 SST anomalies (in °C) in red [blue] for the warm [cold] ENSO years and anomalous area of the warm pool (in million km^2) in red [blue] for anomalous large [small] AWP years are indicated in the brackets of the respective columns of the Table.

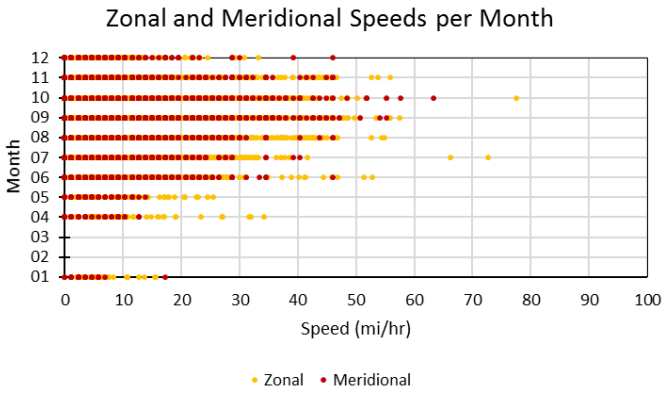

Figure 1: The graph above shows a composite of zonal and meridional TC speeds as a function of month. In general, the zonal component is larger than the meridional, suggesting a slight zonal bias in translation speed.

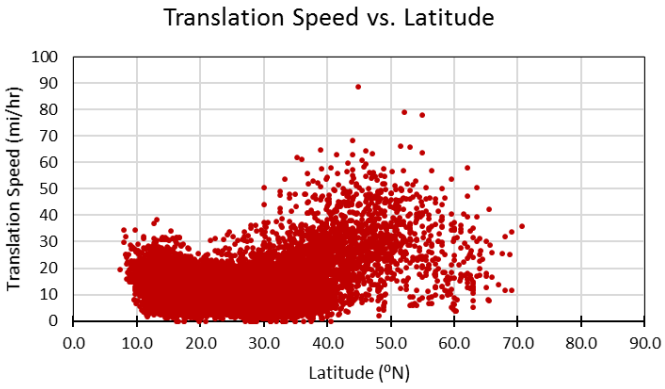

Figure 2: Above is a graph displaying a composite of TC translation speed as a function of latitude.

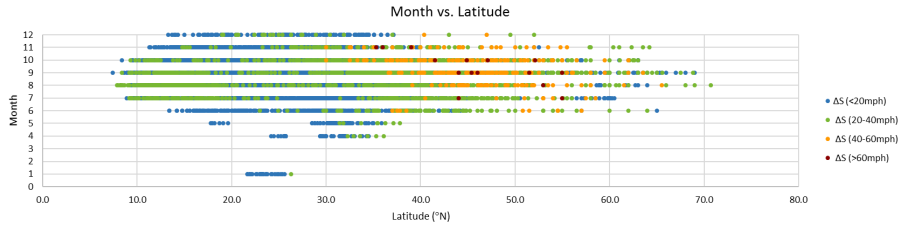

Figure 3: The distribution of the translation speed of North Atlantic TCs as a function of latitude and month of year.

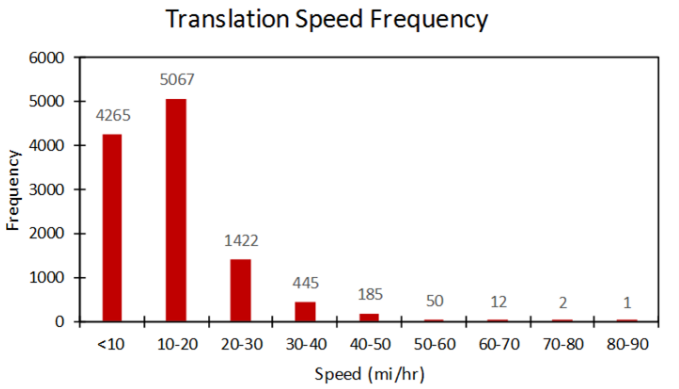

Figure 4: The frequency distribution of translation speeds (mi/hr) of North Atlantic TCs from 1988 to 2014.

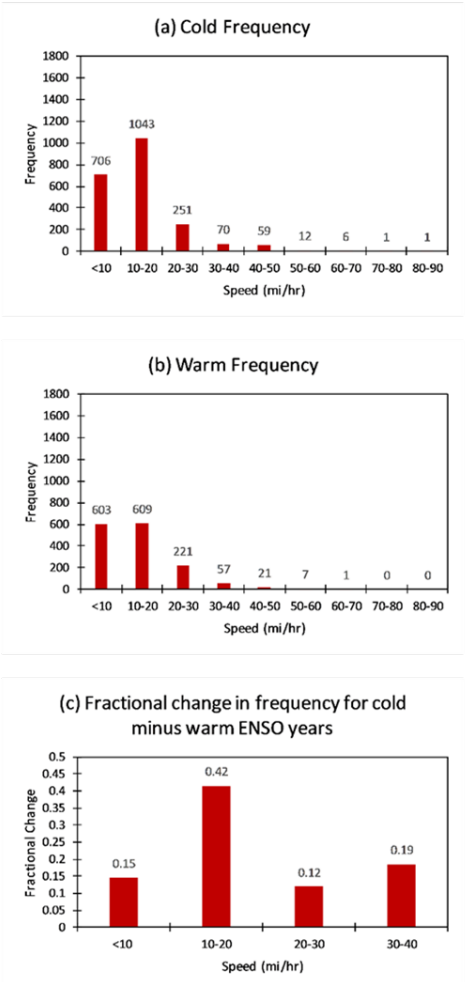

Figure 5: The frequency distribution of translation speed of North Atlantic TCs for a) warm and b) cold ENSO years. c) The fractional change in the frequency of TCs for cold relative to warm ENSO years.

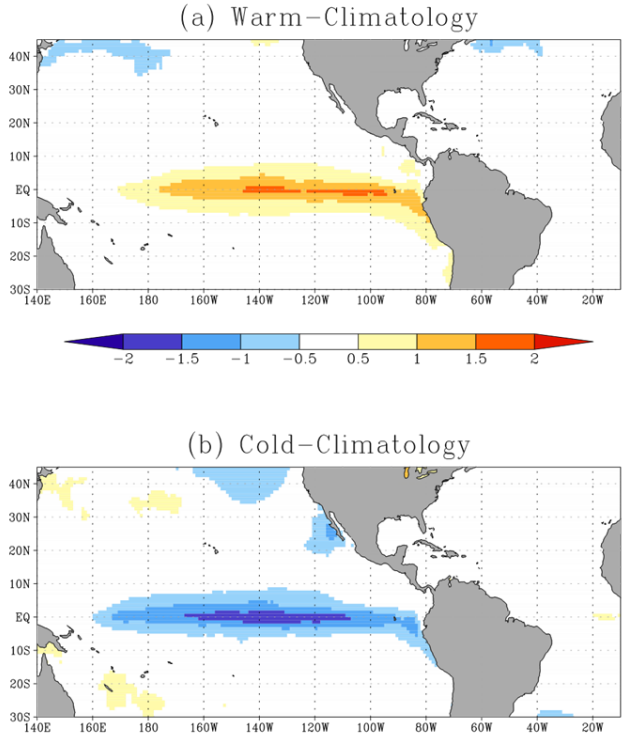

Figure 6: Composites of (June-November) SST anomalies (°C) for a) warm and b) cold ENSO years from OISSTv2 (Reynolds et al. 2007). These years are indicated in Table 2.

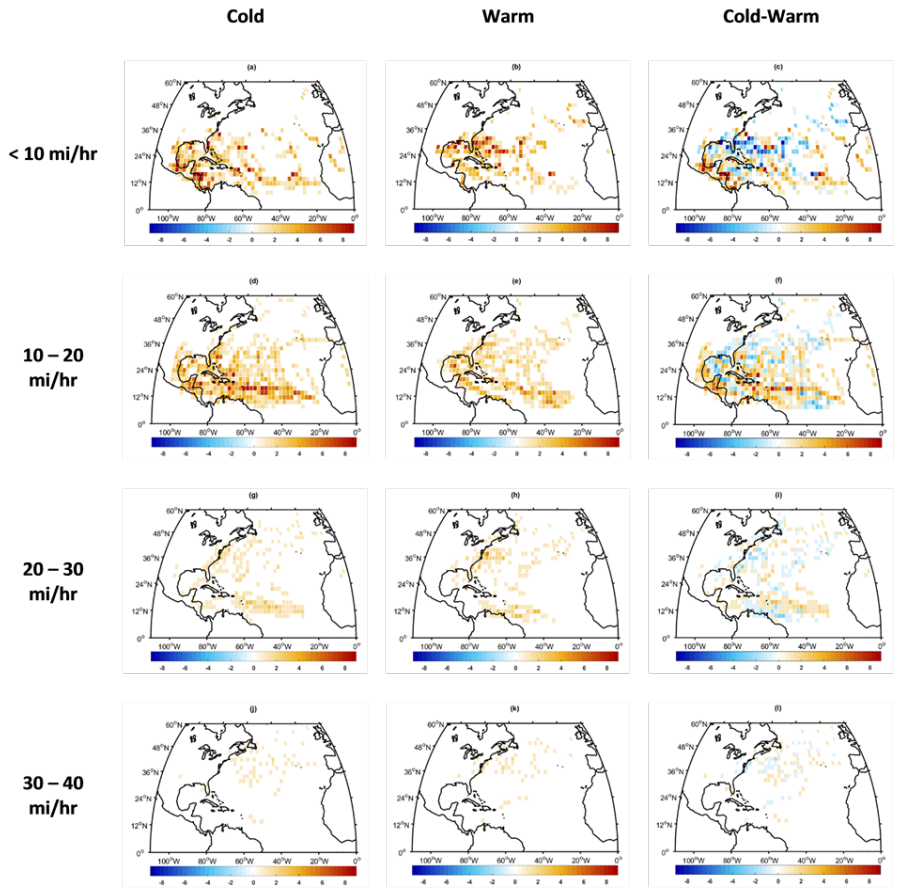

Figure 7: The composite track density (number of TCs per 2°x2° cell) of TC translation speed in the range of a-c) 0-10 mi/hr, d-f) 10-20 mi/hr, g-i) 20-30 mi/hr, and j-l) 30-40 mi/hr for (a, d, g, j) cold, (b, e, h, k) warm, and (c, f, i, l) cold minus warm ENSO years.

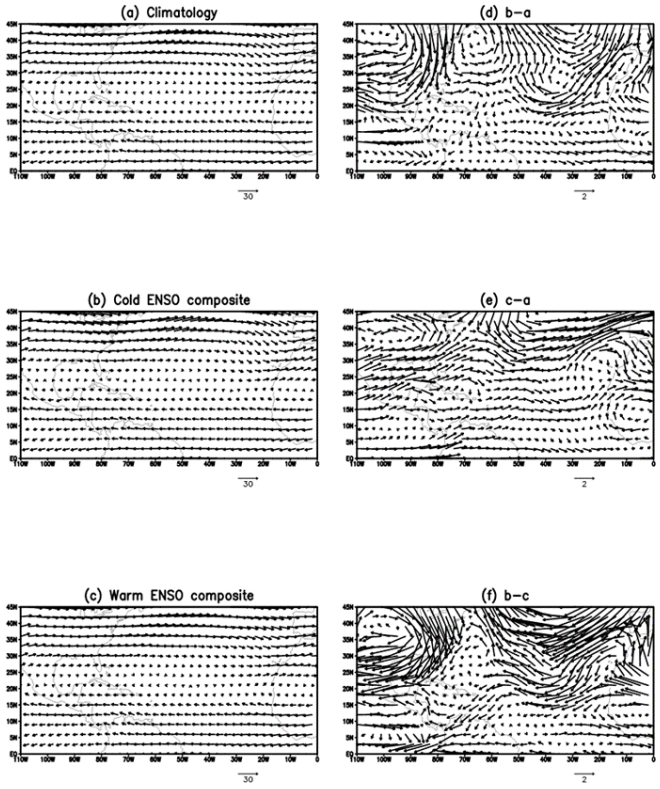

Figure 8: a) The mass weighted climatological steering flow. The mass weighted composite mean steering flow for b) warm and c) cold ENSO years. d) b-a, e) c-a, and f) b-c. The units are in $x10^{-3}$ m/s.

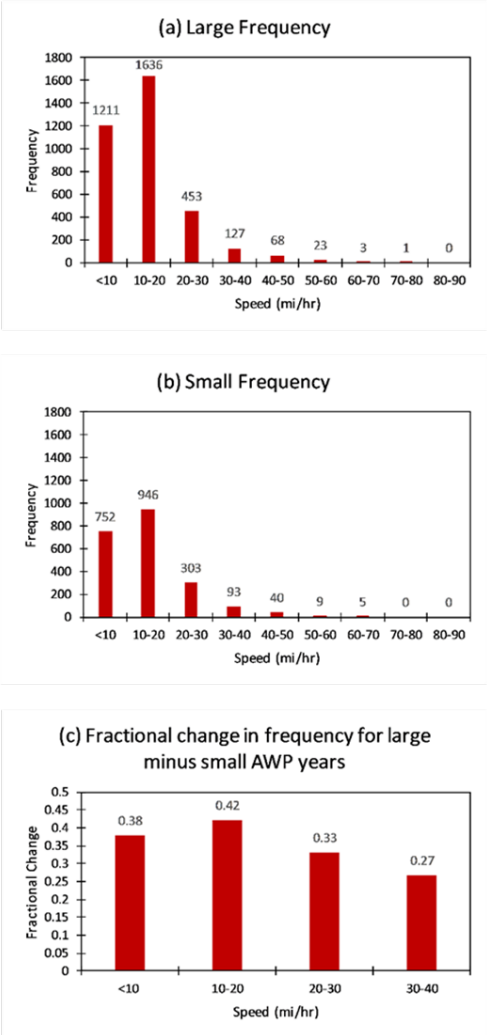

Figure 9: The frequency distribution of translation speed of North Atlantic TCs for a) large and b) small AWP years. c) The fractional change in the frequency of TCs for large relative to small AWP years.

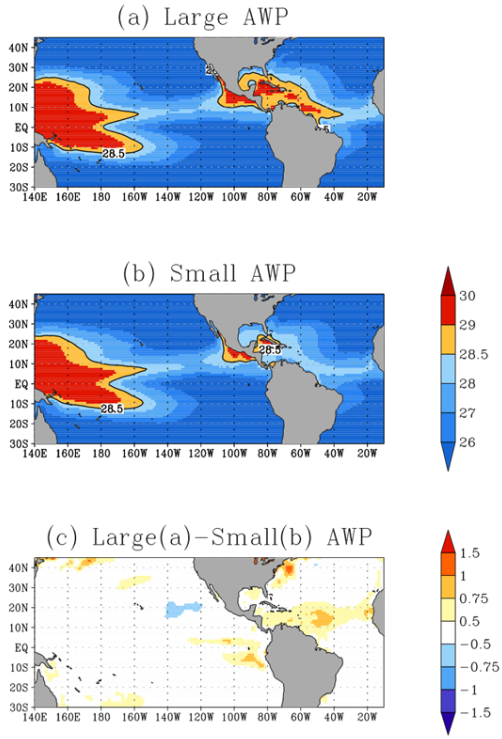

Figure 10: The composite (June-November) SST (in °C) for a) large and b) small AWP years. The years used in the composite are indicated in Table 2. c) (a)-(b).

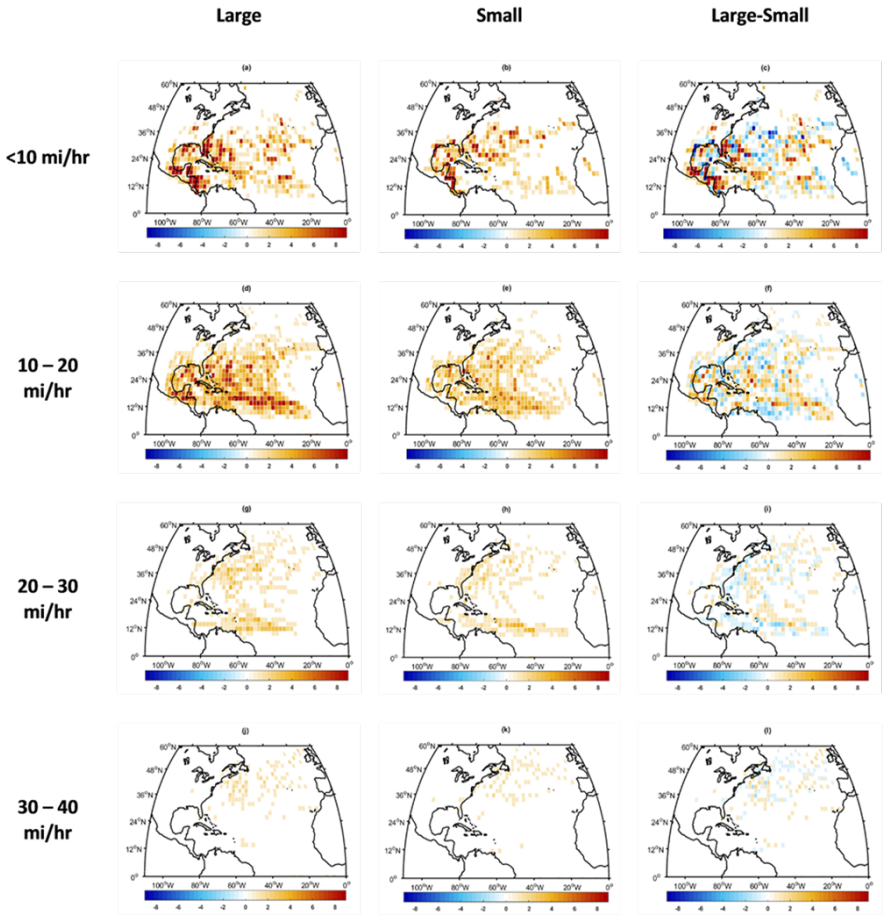

Figure 11: The composite track density (number of TCs per 2°x2° cell) of TC translation speed in the range of a-c) 0-10 mi/hr, d-f) 10-20 mi/hr, g-i) 20-30 mi/hr, and j-l) 30-40 mi/hr for (a, d, g, j) large, (b, e, h, k) small, and (c, f, i, l) large minus small AWP years.

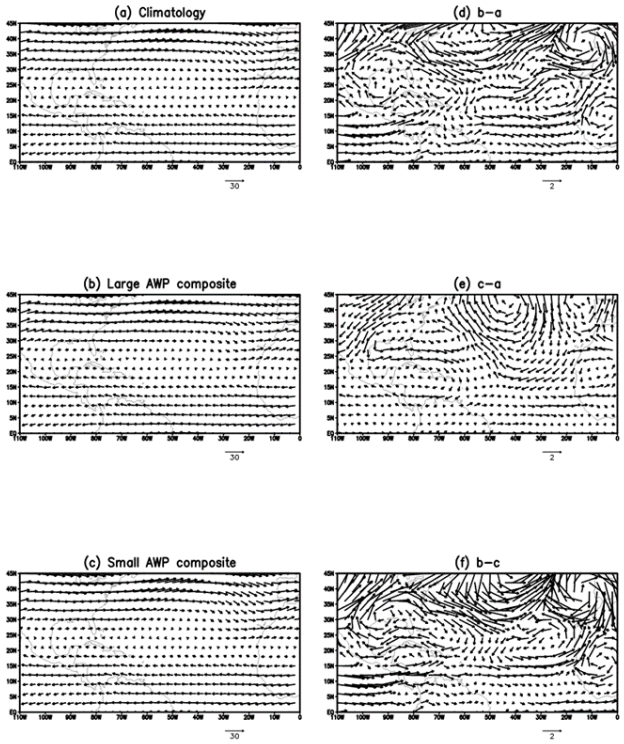

Figure 12: a) The mass weighted climatological steering flow. The mass weighted composite mean steering flow for b) warm and c) cold ENSO years. d) b-a, e) c-a, and f) b-c. The units are in $x10^{-3}$ ms^{-1}.